Astronomical Data Analysis Software and Systems XIII
ASP Conference Series, Vol. 314, 2004
F. Ochsenbein, M. Allen, and D. Egret, eds.

Shadow Bands Observed During the Total Solar Eclipse of 4 December 2002, by High-Resolution Imaging.

Szymon Gladysz, Michael Redfern

Experimental Physics Department, National University of Ireland, Galway, Ireland

Barrie W. Jones

Physics and Astronomy Department, The Open University, Milton Keynes, MK7 6AA, UK

Abstract. We present the results of comparison between characteristics of highly atypical shadow bands recorded during total solar eclipse of 4 December 2002 in Botswana and theory of Codona. For the first time the analysis was based on images of the phenomenon and not photometric data. Thanks to this, use was made of high spatial resolution and detailed plots of power spectra were obtained. The plots' shapes are in excellent agreement with the one predicted by theory. Due to the novel nature of the recording process, some noteworthy image processing techniques were used.

1. Introduction

Shadow bands are natural phenomena that appear just before and just after totality during solar eclipses. They arise from the superposition of atmospheric speckle patterns from elements of an incoherent, extended line source (the remaining visible crescent of the Sun). They are linear patterns moving across the ground with typical speeds of a few m/s in the direction perpendicular to their elongation. They align parallel to the tangent to the centre of the solar crescent (Marschall et al., 1984). It has been observed that shadow band spacing decreases and their contrast increases as totality approaches (Codona, 1986; Jones, 1996, 1999).

2. Obtaining The Data

Shadow bands were recorded during total eclipse of 4 December 2002 in Botswana. The imaging system consisted of a white, diffusely - reflective screen (surface was perpendicular to the line of sight to the eclipsed Sun) and a digital video recorder on a tripod in front of it. For the purpose of observation the aperture was locked fully open, exposure time was 1 ms (so that the phenomenon was "frozen"). The recorder was capturing 25 non-interlaced frames per second.

The bands were also observed visually. They were weak and disorganized and resembled the surface of boiling water rather than linear patterns.

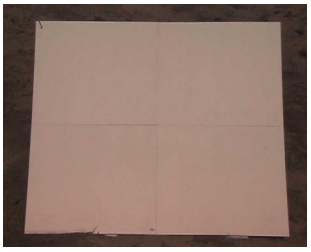

Figure 1. A typical image of the screen. Shadow bands are of extremely low contrast.

3. Image Processing

- Because we could not place the camera between the source and the screen there was a certain amount of perspective elongation that had to be removed from the images (Fig. 1). Perspective transformation arises if a planar object is viewed from a fixed point in space (Glasbey, Mardia, 1998):

$$\begin{aligned} u &= \frac{a_{10}x + a_{01}y + a_{00}}{c_{10}x + c_{01}y + 1}\,, \\ v &= \frac{b_{10}x + b_{01}y + b_{00}}{c_{10}x + c_{01}y + 1} \end{aligned} \tag{1}$$

  where x, y are the coordinates of a point in the object plane, and u, v are the coordinates of the same point in the image plane. The inverse transformation, (u, v) → (x, y), was applied to every image using the reciprocal formulae. The eight parameters ($a_{10}, a_{01}, a_{00}, b_{10}, b_{01}, b_{00}, c_{10}$ *and* c_{01}) were found using known positions of the four corners of the screen before and after the transformation. This meant solving a system of eight linear equations with eight unknowns. Bi-cubic interpolation was used for image scaling.
- Subsequently images were flat-fielded using the ensemble-average as a flat-field. This is a simple variant of a technique proposed by Lindler et al. (1993) for Hubble Space Telescope's Faint Object Spectrograph and usually referred to as 'superflats'. The general decreasing (increasing) trend in overall brightness before (after) totality was removed by normalization. That produced images with the same intensity level as the first (last) image in the sequence. Background around the screen was cropped.
- The intensity values on the screen were in a very small range (30, 40 values on a 0-255 scale). We decided to enhance the contrast by applying Gaussian curve fixing algorithm to the histogram of intensity and this way determining the range that had to be widened (Fig. 2). Afterwards we transformed each value in the histogram to a corresponding new 'bin' between 0 and 255. Thanks to this we achieved values that subtended whole scale.

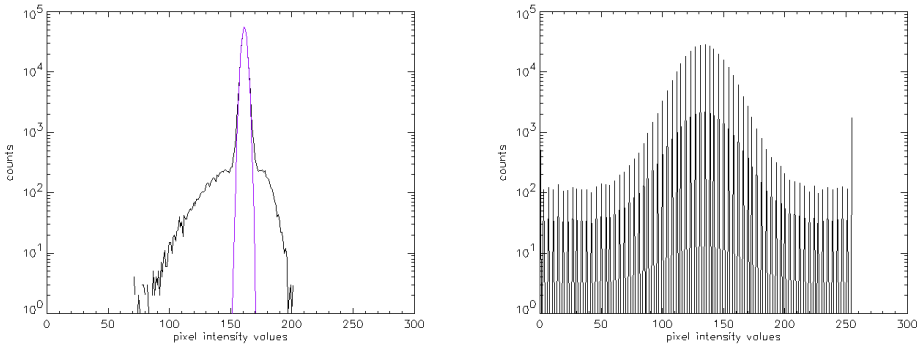

Figure 2. Typical intensity histogram with Gaussian curve fit (left). Histogram of an image after contrast enhancement (right).

4. Results

Two batches of 1480 images (59.2 s) before and after totality were used for further analysis. Operations that could be used to detect shadow bands are:

- computation of the cross-correlation between two successive images to demonstrate the movement of coherent pattern between frames
- application of a FFT algorithm to a single image in order to find the shape of power spectral density function, psd(k), defined by Kay and Marple (1981), as predicted by Codona, and search for shadow bands' characteristic spatial frequencies.

Cross-correlation for different pairs of raw (without contrast enhancement) images revealed nothing but a peak at (0, 0) coordinates. This means that structure of the screen (hardly visible with an un-aided eye) is more pronounced than the shadow bands (meaning zero-shift between the images). Besides that, 25 fps means 40 ms between frames while coherence time (t0) for the atmosphere is usually not more than 10 ms (Monnier, 2003). Shadow bands change their shape too much from one image to another for the cross-correlation to detect them; the temporal-spatial approach was not useful in practice. The theory describing shadow bands is mostly based in the spatial domain, so the use of spatial approach in the analysis is more relevant.

Power spectral density functions were more likely to reveal shadow bands as they are calculated in the spatial domain so that low fps limit of the digital video recorder played no role here. We recorded ambient noise at a low light level with the recorder (same settings as on the observation day), and calculated averaged and normalized psds for the resulting ensemble of images. The psd of an image is a two-dimensional function but for the purpose of this study a one-dimensional psd was calculated in order to make comparisons with Codona's plots. Power spectra for the pixel vectors at a right angle to the tangent to the crescent were calculated separately, added and averaged to produce a psd(k) plot. The psd of the noise was then subtracted from each psd of shadow bands. 60 such functions were computed before and after totality, setting the interval between measurements to 1 s. Smoothing with a rectangular window, 4 pixels wide, was used. The cut-off frequency was imposed by the Nyquist theorem. In

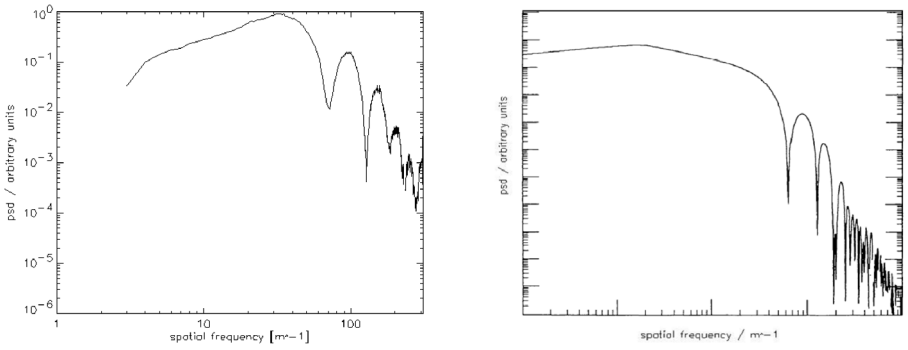

Figure 3. Shadow bands' smoothed psd function (left), 41 s before second contact and Codona's (1986) prediction of a psd(k) shape (right).

some cases noise cancelled the signal in the very low frequency range, but that part of the plots was not significant for further analysis.

The qualitative resemblance between our power spectral density functions and the plot resulting from theoretical assumptions in Codona's paper is striking. According to Codona, shadow bands' psds display three characteristic scales. First characteristic scale is controlled by the geometry of the crescent and corresponds to the low-frequency peak in the spectrum. The next scale relates to the first minimum in the plots and is due to the first null of the source's spectrum. Third scale corresponds to the fast oscillating term in the analytic expression, called the "Fresnel filter" (starting at the second minimum in the plots). Which of them will be the dominant shadow band scale visible to the human eye depends on the distance of the atmospheric scattering layer from the observer and the time to totality. Codona derived formulae relating the height of the scattering layer, z, to the dominant spatial frequency of a psd plot. The derivation of the values of z is the goal of the next stage of the shadow bands' data analysis.

References

Codona, C., 1986. Astronomy and Astrophysics, 164, 415

Glasbey, C. A., Mardia, K. V., 1998. Journal of Applied Statistics, 25, 155

Jones, B. W., 1996. Journal of Atmospheric and Terrestrial Physics, 58, 1309

Jones, B. W., 1999. Journal of Atmospheric and Solar-Terrestrial Physics, 61, 965

Kay, S. M., Marple, S. L., 1981. Proceedings of the IEEE, 69, 1380

Lindler, D., Bohlin, R., Hartig, G., Keyes, C., 1993. FOS Instrument Science Report CAL/FOS-088

Marschall, L. A., Mahon, R., Henry, R. C., 1984. Applied Optics, 23, 4390

Monnier, J. D., 2003. Reports on Progress in Physics, 66, 789